The influence of Ce doping of titania on the photodegradation of phenol

Marcela V. Martin, Paula I. Villabrille & Janina A. Rosso

Environmental Science and Pollution Research

ISSN 0944-1344
Volume 22
Number 18

Environ Sci Pollut Res (2015)
22:14291-14298
DOI 10.1007/s11356-015-4667-4

Springer

Environ Sci Pollut Res (2015) 22:14291–14298
DOI 10.1007/s11356-015-4667-4

RESEARCH ARTICLE

The influence of Ce doping of titania on the photodegradation of phenol

Marcela V. Martin[1] · **Paula I. Villabrille**[2] · **Janina A. Rosso**[1]

Received: 29 December 2014 / Accepted: 6 May 2015 / Published online: 15 May 2015

Abstract Pure and cerium-doped [0.05, 0.1, 0.3, 0.5, and 1.0 Ce nominal atomic % (at.%)] TiO_2 was synthesized by the sol–gel method. The obtained catalysts were characterized by X-ray diffraction (XRD), UV–visible diffused reflectance spectroscopy (DRS), Raman, and BET surface area measurement. The photocatalytic activity of synthesized samples for the oxidative degradation of phenol in aqueous suspension was investigated. The content of Ce in the catalysts increases both the transition temperature for anatase to rutile phase transformation and the specific surface area, and decreases the crystallite size of anatase phase, the crystallinity, and the band gap energy value. The material with higher efficiency corresponds to 0.1 Ce nominal at.%. Under irradiation with 350 nm lamps, the degradation of phenol could be described as an exponential trend, with an apparent rate constant of (9.1 ± 0.6) 10^{-3} s^{-1} (r^2=0.98). Hydroquinone was identified as the main intermediate.

Responsible editor: Philippe Garrigues

✉ Janina A. Rosso
janina@inifta.unlp.edu.ar

Marcela V. Martin
mmartin@inifta.unlp.edu.ar

Paula I. Villabrille
paulav@conicet.gov.ar

[1] Instituto de Investigaciones Fisicoquímicas Teóricas y Aplicadas (INIFTA) CONICET, Universidad Nacional de La Plata (UNLP), La Plata 1900, Argentina

[2] Centro de Investigación y Desarrollo en Ciencias Aplicadas (CINDECA) CONICET, Universidad Nacional de La Plata(UNLP), La Plata 1900, Argentina

Keywords Photocatalysis · Doped titanium dioxide · Cerium · Phenol

Introduction

Phenolic compounds constitute an important family of wastewater pollutants produced by chemical, petrochemical, food-processing, or biotechnological industries (Patel et al. 2014). The current levels of pollutant removal from water, with conventional water treatment technologies, are often not fully satisfactory when wastewater streams contain significant amounts of hardly biodegradable compounds such as phenolic pollutants (Adán et al. 2011).

In recent years, the application of heterogeneous photocatalytic water purification processes has gained wide attention due to its effectiveness in degrading and mineralizing the recalcitrant organic compounds as well as the possibility of utilizing the solar UV and visible-light spectrum. By far, TiO_2 has played a much larger role in this scenario compared to other semiconductor photocatalysts due to its low cost, effectiveness, inert nature, and photostability.

The photocatalytic mechanism is initiated by the absorption of the photon $h\nu$ with energy equal to or greater than the band gap of TiO_2 (~3.1 eV for the anatase phase) producing an electron-hole pair on the surface of TiO_2 particle. An electron is promoted to the conduction band (CB), while a positive hole is formed in the valence band (VB). Excited state electrons and holes can recombine and dissipate the input energy as heat, get trapped in metastable surface states, or react with electron donors and electron acceptors adsorbed on the semiconductor surface or within the surrounding electrical double layer of the charged particles. After the reaction with water, these holes can produce hydroxyl radicals with high redox oxidizing potential. Depending upon the exact conditions, the holes, OH, O_2^-,

H_2O_2, and O_2 itself can play important roles in the photocatalytic reaction mechanism (Grabowska et al. 2012).

A substantial amount of research has focused on the enhancement of TiO_2 photocatalysis by modification with metal, nonmetal, and ion doping (Pelaez et al. 2012; Grabowska et al. 2012; Daghrir et al. 2013). The primary purposes of doping TiO_2 are to retard the fast charge recombination and enable visible light absorption by creating defect states in the band gap. Generally speaking, the photocatalytic activities of TiO_2 depend on various parameters in a complex way. Not only the intrinsic properties of TiO_2 (e.g., crystallinity, surface area, particle size, defect sites, surface charge) but also the substrate–surface interactions that should depend on the kind of substrate play significant roles in deciding the overall photocatalysis (Park et al. 2013).

Doping with lanthanides is a promising choice since lanthanide ions are known for their ability to form complexes with various Lewis bases (e.g., alcohols, aldehydes, amines, etc.) through the interaction of these functional groups with the *f* orbitals of lanthanides (Ranjit et al. 2001). Moreover, rare earth oxides are found to have polymorphs, strong adsorption selectivity, good thermal stability, etc., due to their *f* electron and multi-electron configuration (Xu et al. 2006).

Particularly, the utilization of Ce-doped TiO_2 was reported for the degradation of some substrates: 2-mercaptobenzothiazole (Li et al. 2005), rhodamine B (Xiao et al. 2006), formaldehyde (Xu et al. 2006), 4-chlorophenol (Silva et al. 2009), methylene blue (Aman et al. 2012), and bisphenol A (Chang and Liu 2014). The efficiencies of these treatments were diverse, as expected, because the process is substrate-dependent.

Several reviews focus on comparing the efficiency of different treatments for the degradation of phenol as a "model" contaminant (Esplugas et al. 2002; Liotta et al. 2009; Grabowska et al. 2012). However, no reports were found about the influence of cerium doping of TiO_2 on the photodegradation of phenol.

We present here a comparative study on the photocatalytic efficiency of undoped and Ce-doped TiO_2 (0.05–1.0 Ce nominal at.%) prepared by the sol–gel method. The synthesized samples were characterized by X-ray diffraction, Raman scattering, UV-visible diffuse reflectance spectra, and N_2 physisorption. The photocatalytic activity of the materials for the oxidative degradation of phenol in aqueous suspension, under different irradiation sources, was investigated.

Experimental section

Chemicals

The following specific reagents were used in this study: titanium tetraisopropoxide (TTIP, Aldrich), absolute ethanol (Anedra), nitric acid (Anedra), titanium dioxide (Degussa P25), and phenol (Aldrich). The metal-ion precursor used in the preparation was cerium(III) nitrate hexahydrate ($Ce(NO_3)_3.6H_2O$, Aldrich).

Preparation of photocatalysts

The photocatalysts were prepared by standard sol-gel methods. TiO_2 sols were obtained by dropwise addition of an ethanolic TTIP solution, where 5 mL of TTIP was mixed with 50 mL of anhydrous ethanol, to 50 mL of distilled water adjusted to pH 1 with nitric acid under vigorous stirring at 25 °C. After continuously stirring for 24 h, the resulting suspension was evaporated and dried at 50 °C overnight. The obtained crystals were ground to powder and calcined at 400 °C (6 °C min^{-1}) or 600 °C (6 °C min^{-1}) for 1 h, under air. Ce-doped TiO_2 samples were prepared according to the above procedure in the presence of $Ce(NO_3)_3$ $6H_2O$ to give a doping level from 0.05 to 1.0 nominal at.%. The appropriate amount of metal-ion precursor was added to distilled water before the hydrolysis of TTIP, and the subsequent procedures were the same as described above. The undoped sample is white, while the doped samples exhibited different tones of yellow according to their Ce content. The prepared materials calcined at 600 °C will be referred to hereafter as undoped and 0.05 Ce, 0.1 Ce, 0.3 Ce, 0.5 Ce, and 1.0 Ce (referring to Ce nominal at.%). Similarly, the catalysts calcined at 400 °C will be referred to as undoped-400 and 0.1 Ce-400.

Characterization of the photocatalysts

Crystal structure patterns of the Ce-doped TiO_2 powder samples were examined by X-ray diffraction (XRD) using a Philips diffractometer (PW-1390) with Cu Kα radiation. The Raman scattering measurements of TiO_2 samples were performed in the backscattering geometry at room temperature in air using a Jobin-Yvon T64000 triple spectrometer, equipped with a confocal microscope and a nitrogen-cooled charge-coupled device detector. The spectra were excited by a 514.5 nm line of argon laser with an output power of less than 5 mW to avoid local heating due to laser irradiation. Brunauer-Emmett-Teller (BET) surface area measurements were carried out using N_2 as the adsorptive gas (Micromeritics ASAP 2020). UV–Vis diffuse reflectance spectra (DRS) were obtained on a UV–Vis Perkin-Elmer Lambda 35 spectrophotometer.

Photocatalytic decomposition of pollutant

The photocatalytic oxidation of phenol in catalyst suspensions was carried out in a glass reactor at 25 °C, in air and with continuous stirring to ensure that the material was in suspension. For each run, the reaction mixture was prepared by ultrasonically dispersing 100 mg catalyst, 5 μg phenol

(Aldrich), and 100 mL ultrapure water (Milli-Q: resistivity >18 MΩ cm and <20 ppb organic carbon), in the dark for 15 min. A Rayonet photochemical reactor RPR-100 (Southern New England Ultraviolet Company) with interchangeable lamps of different wavelengths (white, 350 or 575 nm) was used. The corresponding spectra are shown in Fig. 1.

The sampling was performed periodically. The phenol concentration and intermediate products (catechol, hydroquinone and *p*-benzoquinone) in the filtered samples were determined by HPLC (HP 1050 Ti series) using the corresponding standard solutions. The elution was monitored at wavelengths of 200, 270, 200, and 250 nm for phenol, catechol, hydroquinone, and *p*-benzoquinone, respectively. The column was a C18 Restek Pinnacle II (particle size 5 μm, 2.1 mm, id 250 mm), and the mobile phase was a 50/50 (*v*/*v*) methanol/H_3PO_4 (0.2 %) mixture at 0.1 mL min^{-1} constant flux.

The evolution of phenol concentration in aqueous solution with irradiation (without catalyst) and without irradiation (but with each catalyst) was performed to check direct photolysis and the adsorption of phenol on the materials, respectively.

To analyze the Ce and Ti leaching from the catalysts, metal ion concentrations were determined using ICP-mass spectrometry (ICP-MS, Nexlon 300X, Perkin-Elmer Co., USA). The sampling was performed at the end of the irradiation period. The samples were filtered through a cellulose membrane with pore size of 0.45 μm and stored in the refrigerator until analysis.

Results and discussion

Catalyst characterization

Figure 2 shows XRD patterns of undoped and modified TiO_2 photocatalysts. It was found that all samples calcined at 400 °C were of anatase phase. Compared to highly crystalline anatase TiO_2, (103) and (112) crystal faces did not grow very well, which commonly occurred in TiO_2 calcined below 500 °C (Sun et al. 2013).

An increase in calcination temperature to 600 °C resulted in a significant improvement in the crystallinity of the material. For undoped titania, a complete A–R (anatase to rutile) transformation was observed. The presence of both phases, anatase (A) and rutile (R), in doped material with a low nominal amount of Ce (0.05 Ce, 0.1 Ce, and 0.3 Ce) was detected, while for 0.5 Ce and 1.0 Ce, only the A phase was observed. This result indicates that the presence of Ce inhibited the phase transformation at 600 °C. The chemical bonds of Ti–O–Ce three elements around the anatase crystallites could easily occur during the thermal treatment process, which possibly inhibited the formation and growth of the crystal nucleus of rutile (Liqiang et al. 2004).

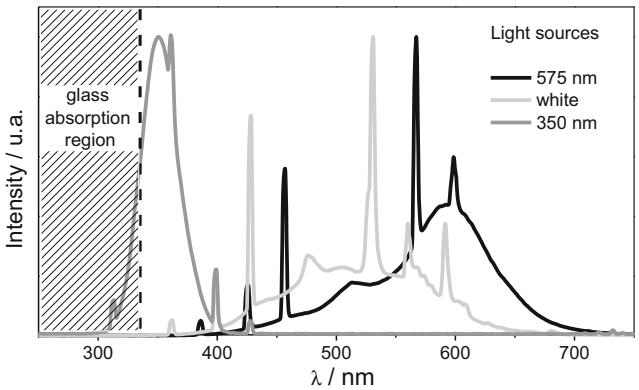

Fig. 1 Emission spectra of light sources and reactor glass absorption region

Moreover, as the content of Ce increased in the doped samples, the peaks broadened, and their intensity slightly weakened indicating weaker crystallinity. Lanthanide ions are known to be less reactive than titania precursor species, which also slows down the condensation and crystallization processes of the titania matrix (Aman et al. 2012).

No diffraction peaks that could be attributed to the dopant ion were observed, not even for the highest Ce content. Our result suggests that the doping levels or the thermal treatment employed does not induce the formation of discrete impurity phases of cerium oxide, in accordance with a previous report (Aman et al. 2012). Furthermore, the ionic radius of Ce^{3+} is 0.097, which is much larger than that ofTi^{4+} (0.061 nm) but smaller than that of oxygen (0.14 nm). Hence, it is difficult for lanthanide ions to enter the TiO_2 lattice to replace Ti^{4+} ions (Nguyen-Phan et al. 2009). It is conceivable that metal impurities, which were formed during synthesis, were nanoscopic or possibly well dispersed on the surface (Choi et al. 2010).

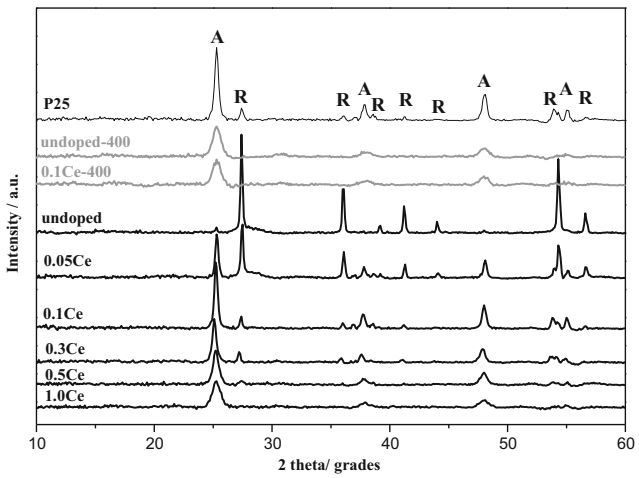

Fig. 2 XRD patterns of undoped and Ce-doped TiO_2 samples (calcined at 600 °C), undoped-400, and 0.1 Ce-400 (calcined at 400 °C) compared with P25 Degussa

The diffraction peak broadening was used to estimate the average TiO_2 crystallite size in terms of the Scherrer equation (Klug and Alexander 1974):

$$D = K\lambda/\beta\cos\theta$$

where D is the average crystallite diameter in angstrom, β is estimated as the line width at half-maximum height of the main intensity diffraction peak of anatase (101) or rutile (110) after background removal, K=0.89 is a constant related to the crystallite shape and the way in which D and β are defined, θ is the diffraction angle, and λ is the X-ray wavelength corresponding to CuKα irradiation (1.5417 Å).

The XRD intensities of the anatase (101) peak and the rutile (110) peak were also analyzed. The weight percent of the anatase and rutile phases was determined by Spurr–Myers equation (Demeestere et al. 2005):

$$A\ \text{wt\%} = \left(1 + 1.265 I_R/I_A\right)^{-1} \times 100$$
$$R\ \text{wt\%} = 100 - A\ \text{wt\%}$$

I_A and I_R refers to the diffraction intensities of the (101) anatase and (110) rutile crystalline phases at 2θ=25.3° and 27.5°, respectively.

The crystallite sizes of anatase and rutile at each calcination temperature are listed together with their respective percentages in Table 1.

The crystallite size of anatase thus estimated for samples calcined at 400 °C was 10.12 nm for undoped titania, while there was no change in size after doping with 0.1 at.% Ce. For samples calcined at 600 °C, A crystallite size decreases from 26.32 nm (0.05Ce) to 9.05 nm (1.0 Ce). The presence of relatively large Ce^{3+} on the particle surfaces, at grain boundaries and grain junctions, could inhibit the crystallite growth of titania through the formation of Ce–O–Ti bonds that increase the diffusion barrier at the titania grain junctions (Sibu et al. 2002).

Raman spectra were further employed to identify the surface geometric structure of the samples. As shown in Fig. 3, three Raman-active modes corresponding to the typical vibrational bands of rutile TiO_2 (Ma et al. 2007; Yan et al. 2014) are clearly observed for undoped TiO_2 calcined at 600 °C.

For the doped materials, the Raman spectra of the catalysts calcined at 600 °C are dominated by anatase Raman modes (Ohsaka et al. 1978; Grujić-Brojčin et al. 2014): $E_{g(1)}$ (140 cm^{-1}), $E_{g(2)}$ (195 cm^{-1}), B_{1g} (395 cm^{-1}), A_{1g} + B_{1g} (518 cm^{-1}), and $E_{g(3)}$ (636 cm^{-1}), as shown in the inset of Fig. 3.

Nitrogen adsorption–desorption isotherms of prepared photocatalyst samples were tested to evaluate the textural properties. Adsorption isotherms of certain selected compositions, calcined at 400 and 600 °C, are presented in Fig. 4.

All the isotherms exhibited typical type IV behavior with a hysteresis loop caused by capillary condensations within the mesopores, according to BDDT (Brunauer–Deming–Deming–Teller) classification (Sing et al. 1985). Average pore diameters obtained from BJH desorption were 9.2 and 8.1 nm for undoped and 1.0 Ce, respectively. Volume adsorption was higher for Ce-doped than for the undoped sample, which indicates a higher surface area. Moreover, it was found that the specific surface area increases from 4.75 m^2/g for the undoped sample to 57.71 m^2/g for the Ce-doped samples (see Table 1). Considering the XRD results of the Ce-doped sample, it can be concluded that the doping of Ce ions can confine the crystallite size, which results in the larger specific surface area of Ce-doped samples.

According to the BET analysis for the 0.1 Ce sample, the rise in calcination temperature reduces the surface

Table 1 Structural, textural, and optical properties of synthesized photocatalysts calcined at 600 and 400 °C, and commercial P25 for comparison

Photocatalyst	XRD				Nitrogen physisorption	UV–Vis
	Crystallite size[a] (nm)		Crystalline phase[b] (wt.%)		BET surface area (m^2/g)	Absorption edge (eV)
	Anatase	Rutile	Anatase	Rutile		
P25	21.32	54.17	76	24	81.88	3.16
undoped	n.d.	98.47	n.d.	100	4.75	3.07
0.05Ce	26.32	82.72	39	61	16.37	3.06
0.1Ce	23.86	84.40	81	19	27.68	2.80
0.3Ce	20.69	56.90	72	28	33.35	2.75
0.5Ce	13.57	n.d.	100	n.d.	42.94	2.70
1.0Ce	9.05	n.d.	100	n.d.	57.71	2.68
undoped-400	10.12	n.d.	100	n.d.	87.42	3.02
0.1Ce-400	10.11	n.d.	100	n.d.	83.92	2.90

[a] Estimated by Scherrer equation using the XRD line broadening

[b] Weight percent of anatase and rutile were calculated by Spurr–Myers equation.

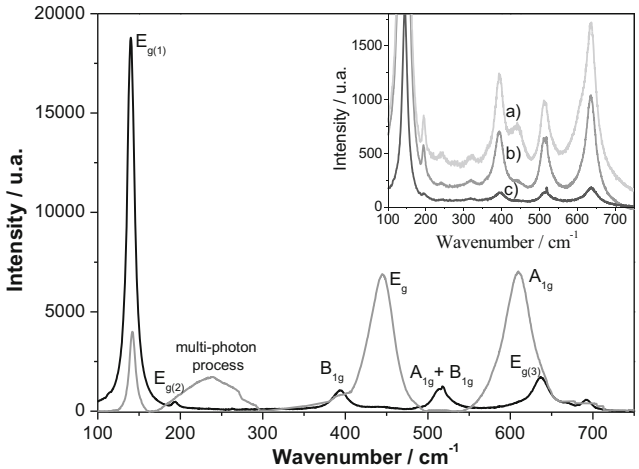

Fig. 3 The Raman spectra of the P25 (black) and undoped TiO_2 calcined at 600 °C (*gray*) catalysts. *Inset graph*. Raman spectra of the following: **a** 0.1 Ce, **b** 0.3 Ce, and **c** 1.0 Ce samples (calcined at 600 °C)

area from 83.92 m^2/g (400 °C) to 27.68 m^2/g (600 °C), to the detriment of the amount of active sites on which the reactants can be adsorbed. However, powders with a large surface area are usually associated with large amounts of crystalline defects, which favor electron-hole recombination leading to a poor photoactivity. Recently, it has been reported that the photocatalytic activity of amorphous TiO_2 is negligible, indicating that crystallinity is an important requirement. Then, a balance between surface area and crystallinity must be found in order to obtain the highest photoactivity (Carp et al. 2004).

The absorption spectra of the samples were evaluated by UV–Vis DRS as shown in Fig. 5. Prepared undoped TiO_2 showed an absorption threshold at 410 nm, which is characteristic of the rutile phase (Yan et al. 2014). Cerium incorporation to TiO_2 induces a red shift of the electronic absorption band that correlates with the Ce

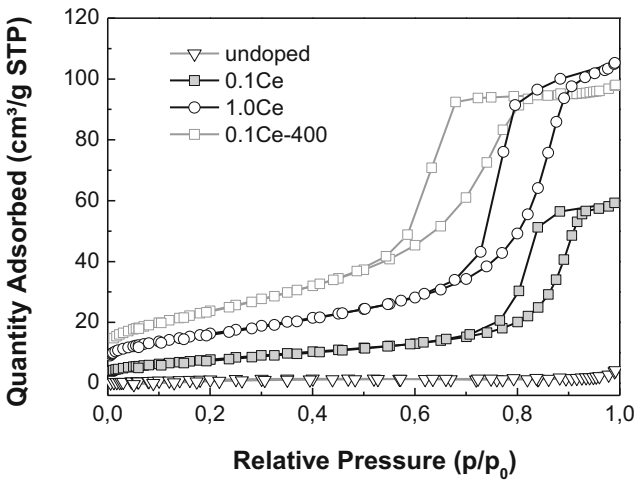

Fig. 4 N_2 sorption isotherms at 77 K on undoped TiO_2, 0.1 Ce, and 1.0 Ce samples (calcined at 600 °C) and 0.1 Ce-400 (calcined at 400 °C)

content of the material. Such observation is consistent with previous studies (Coronado et al. 2002; Xiao et al. 2006). This redshift of the absorption edge in Ce-doped catalysts promotes the generation of electron-holes under visible-light irradiation.

The band gap energies of the materials could be estimated using the following equation (Zhou et al. 2011):

$$(\alpha h\nu)^n = B(h\nu - Eg)$$

where $h\nu$ is the photon energy, α is the absorption coefficient that can be obtained from the scattering and reflectance spectra according to the Kubelka–Munk theory, B is a constant relevant to the material, and n is the value that depends on the nature of transition: 2 for a direct allowed transition, 3/2 for a direct forbidden transition, and 1/2 for an indirect allowed transition. The $(\alpha h\nu)^n$ (n=1/2) versus $h\nu$ extrapolated to α=0 represents the absorption band gap energy. Table 1 lists the band gap energy values of the TiO_2 photocatalysts. The band gap energy for the undoped TiO_2 is 3.07 eV and decreases with Ce content up to 2.68 eV (for 1.0 Ce).

Photocatalytic degradation of phenol

The evolution of phenol concentration in aqueous solution with irradiation (without catalyst) and without irradiation (but with each catalyst) was performed as control experiments. Neither of them presents degradation of phenol. Moreover, no significant adsorption effect was observed (by comparison with analytical concentration).

Experiments of photocatalytic degradation of phenol using three different light sources (white, 350 and 575 nm) were done. Figure 6 shows the percentage of degradation after 3 h (with 350 nm lamp) and 5 h (with white and 575 nm lamps) of irradiation.

The efficient absorption of visible light does not appear to be a decisive factor in the photocatalytic activity of Ce-TiO_2. Although the catalyst absorption at λ >400 nm increases with the Ce content (see Fig. 5), the irradiation with specific sources of light did not yield a better efficiency of photocatalytic degradation. This observation is in line with the behavior described by other authors (Li et al. 2005; Choi et al. 2010). However, due to the relevance of visible light in the solar spectrum, the degradation of 25 % of the initial concentration of phenol by 0.1 Ce is a promising result.

For the three lamps used, the addition of a low amount of cerium to the catalysts (0.05 %) increases the percentage of degradation of phenol compared to undoped material. However, when the 0.1 Ce at.% (0.6 % *w*/*w*) is exceeded, the efficiency stays the same or decreases. This decrease in the photocatalytic activity of Ce-doped catalysts with the increment of Ce concentration above certain values was already

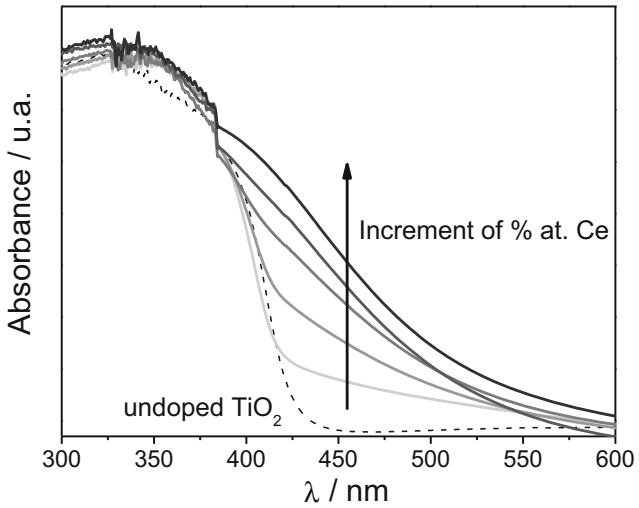

Fig. 5 UV–visible diffuse reflectance spectra (DRS) for the synthesized catalysts (calcined at 600 °C)

observed and was attributed to the presence of amorphous phase, promoting electron-hole recombination (Silva et al. 2009).

We found that 0.05 Ce, 0.1 Ce, and 0.3 Ce with both phases (A and R) were better materials for the degradation of phenol. A similar observation, namely that the mixtures of both phases exhibit higher photoactivity as well as effective degradation of phenol in comparison with pure A or R catalysts, was reported for pure TiO_2 (Zhang et al. 2000). Moreover, it was reported (Choi et al. 2010) that metal-doped TiO_2 with a relatively high fraction of rutile (around 28 %) showed significantly enhanced photocatalytic activity (evaluated for methylene blue degradation, iodide oxidation, and phenol degradation under visible-light irradiation at λ >400 nm).

Recently, Wang et al. (2014) reported that an increase in the crystallite size from 6.6 to 26.6 nm led to a significant improvement in the photoreactivity of pristine anatase nanoparticles (for the degradation of phenol), while this reactivity was independent of the crystallinity. Interestingly, our best performing catalysts (0.05 Ce, 0.1 Ce and 0.3 Ce) have A crystallite sizes (see Table 1) similar to the better value reported there (Wang et al. 2014). Therefore, the relation of A/R phases seems to be as important as the crystallite size in the photoreactivity of TiO_2 catalysts.

A closer study was performed with the 0.1 Ce catalyst (the better synthesized material). The catalyst stability is essential for industrial applications since it has to maintain its activity during a long period of operation. One of the main drawbacks of metallic catalysts is the leaching of the active phase into the liquid phase (Martins et al. 2010). The concentrations of Ti and Ce, after the utilization of the catalyst, were determined in the reaction mixture. For both metals, the values were under the detection limits, 5 ppb (for Ti) and 70 ppt (for Ce). Then, the photocatalytic activity could be considered as a heterogeneous process.

For the three light sources, the degradation of phenol (with 0.1Ce) followed an exponential trend. The apparent rate constants were (7.0±0.3) 10^{-4} s^{-1} (r^2=0.99), (9.6±0.1) 10^{-4} s^{-1}

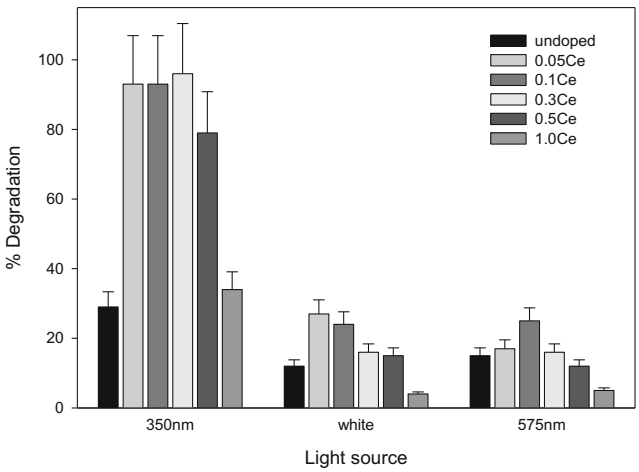

Fig. 6 Percentage of phenol degradation with the prepared catalysts, after 3 h (with 350 nm lamp) and 5 h (with white and 575 nm lamps)

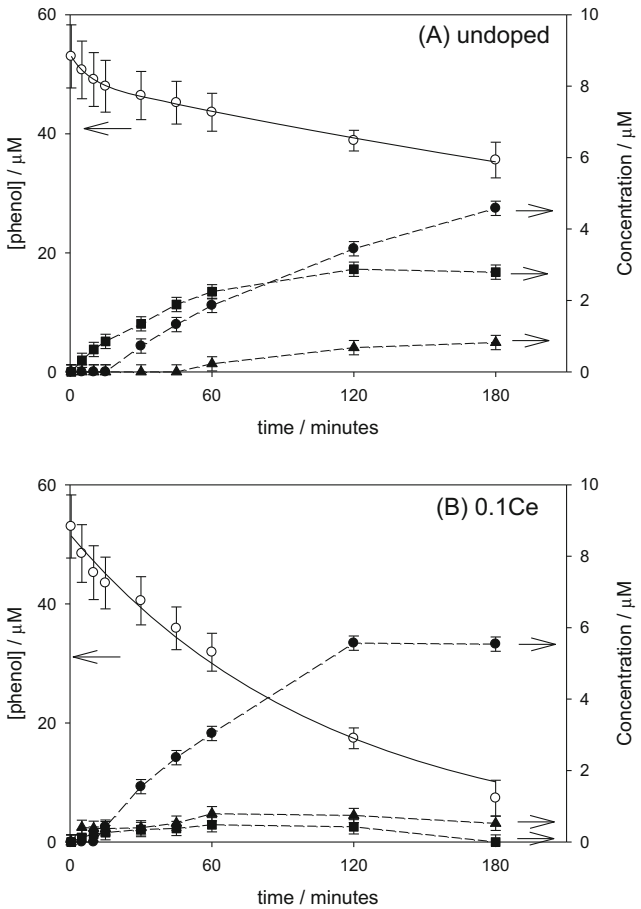

Fig. 7 Phenol degradation with undoped (**a**) and 0.1 Ce (**b**) catalysts, after 3 h with 350 nm lamps (*white circle*, left axis) and intermediates detected (*right axis*): hydroquinone (*black circle*), catechol (*black square*), and *p*-benzoquinone (*black triangle*). $[phenol]_0$=53 μM, 1 g L^{-1} of catalyst, air-saturated mixtures

(r^2=0.99), and (9.1±0.6) 10^{-3} s^{-1} (r^2=0.98) for white, 575 and 350 nm lamps, respectively. This observation is in line with reported behaviors for pristine anatase TiO_2 (Wang et al. 2014) and Degussa P25 TiO_2 with 80 % A and 20 % R (Peiró et al. 2001). However, the degradation of phenol by undoped TiO_2 (calcined at 600 °C) could be described as bi-exponential decay, indicating a more complex mechanism. The absence of the A phase in this material (it is only R) may be responsible for this difference.

For undoped and 0.1 Ce catalysts with 350 nm irradiation, three main intermediates were detected: hydroquinone, catechol, and *p*-benzoquinone, all reported as oxidative products of phenol (see Fig. 7).

For pure TiO_2 (in the form of A or a mixture of A and R) excited by UV irradiation, OH radicals are a primary oxidation species responsible for phenol degradation or mineralization. The attack of the electrophilic radical OH occurs at the ring positions activated by the presence of the substituent. The phenolic –OH group is electron-donating for the electrophilic aromatic substitution, then the electron density at the *ortho* and *para* positions increases. Hydroquinone and catechol are the main intermediates from this attack (Di Paola et al. 2003). The *p*-benzoquinone can be formed in three different ways: (i) by OH attack on the hydroquinone molecule; (ii) in the reaction of that molecule with holes photogenerated in titanium dioxide; and (iii) by oxidation of hydroquinone by oxygen dissolved in water (Grabowska et al. 2012). Catechol, similarly to hydroquinone, forms *o*-benzoquinone. The compound is, however, very unstable and hence its absence in the detected products of photochemical oxidation of phenol or catechol (Grabowska et al. 2012).

In our experiments with the undoped catalyst, the amount of hydroquinone was 7.6 %, that of catechol, 5.3 % and *p*-benzoquinone, 1.4 % (assuming 100 % for initial phenol concentration). The presence of both dihydroxylated intermediates indicates the OH radical attack, as expected.

In the case of metal-doped TiO_2 excited by visible light, both OH radicals and direct oxidation could be employed (Grabowska et al. 2012). Moreover, lanthanide interacts strongly with the aromatic ring, and this interaction encourages the direct oxidation through the positive hole present on the surface (Silva et al. 2009). However, no significant adsorption of phenol on the 0.1 Ce catalyst was observed, making the contribution of direct oxidation in our studies less important.

In the experiments with 0.1 Ce, a pronounced increase in the degradation rate of phenol was observed. Since cerium extends the photoresponse into the visible region, this can lead to an increase in the charge separation efficiency of surface electron-hole pairs. The redox pair of cerium (Ce^{3+}/Ce^{4+}) is also important, since cerium could act as an effective electron scavenger to trap the bulk electrons in TiO_2 (Silva et al. 2009).

Under 350 nm irradiation, the utilization of 0.1 Ce catalyst yielded hydroquinone as the main intermediate (10.5 %, assuming 100 % for initial phenol concentration). Then, we propose the OH radicals attack phenol and the primary intermediates. As a consequence of these attacks, only a residual concentration of hydroquinone was detected after 3 h of treatment.

Conclusion

It can be concluded that the increasing level of cerium in the material (i) increases the transition temperature for anatase to rutile phase transformation, (ii) confines the crystallite size of anatase phase, (iii) increases the specific surface area, (iv) decreases the crystallinity, and (v) induces a red shift of the electronic absorption band.

However, no direct correlation between these characteristics and the photocatalytic activity was found. The material with higher efficiency corresponds to 0.1 Ce nominal at.%. Under irradiation with 350 nm lamps, the degradation of phenol could be described as an exponential trend, with an apparent rate constant of (9.1±0.6) 10^{-3} s^{-1} (r^2=0.98). Hydroquinone was identified as the main intermediate.

Acknowledgments This work was supported by Grant PICT 2011 0832 from Agencia Nacional de Promoción Científica y Tecnológica, (ANPCyT, Argentina). J.A.R. and P.I.V. are research members of CONICET (Consejo Nacional de Investigaciones Científicas y Tecnológicas de la República Argentina). M.V.M. thanks CONICET for a postdoctoral studentship. The authors wish to thank E. Soto for his experimental contribution for N_2physisorption measurements.

References

Adán C, Carbajo J, Bahamonde A, Ollerb I, Malato S, Martínez-Arias A (2011) Solar light assisted photodegradation of phenol with hydrogen peroxide over iron-doped titania catalysts: role of iron leached/readsorbed species. Appl Catal B: Environ 108–109:168–172

Aman N, Satapathy PK, Mishra T, Mahato M, Das NN (2012) Synthesis and photocatalytic activity of mesoporous cerium doped TiO_2 as visible light sensitive photocatalyst. Mater Res Bull 47:179–183

Carp O, Huisman CL, Reller A (2004) Photoinduced reactivity of titanium dioxide. Prog Solid State Ch 32(33):17

Chang S-M, Liu W-s (2014) The roles of surface-doped metal ions (V, Mn, Fe, Cu, Ce, and W) in the interfacial behavior of TiO_2 photocatalysts. Appl Catal, B 156–157:466–475

Choi J, Park H, Hoffmann MR (2010) Effects of single metal-ion doping on the visible-light photoreactivity of TiO_2. J Phys Chem C 114: 783–792

Coronado JM, Maira AJ, Martinez-Arias A, Conesa JC, Soria J (2002) EPR study of the radicals formed upon UV irradiation of ceria-based photocatalysts. J Photoch Photobio A 150:213–221

Daghrir R, Drogui P, Robert D (2013) Modified TiO_2 for environmental photocatalytic applications: a review. Ind Eng Chem Res 52:3581–3599

Demeestere K, Dewulf J, Ohno T, Herrera Salgado P, Van Langenhove H (2005) Visible light mediated photocatalytic degradation of gaseous trichloroethylene and dimethyl sulfide on modified titanium dioxide. Appl Catal B: Environ 61:140–149

Di Paola A, Augugliaro V, Palmisano L, Pantaleo G, Savinov E (2003) Heterogeneous photocatalytic degradation of nitrophenols. J Photoch Photobio A 155:207–214

Esplugas S, Gimenez J, Contreras S, Pascual E, Rodriguez M (2002) Comparison of different advanced oxidation processes for phenol degradation. Water Res 36:1034–1042

Grabowska E, Reszczynska J, Zaleska A (2012) Mechanism of phenol photodegradation in the presence of pure and modified-TiO_2: a review. Water Res 46:5453–5471

Grujić-Brojčin M, Armaković S, Tomić N, Abramović B, Golubović A, Stojadinović B, Kremenović A, Babić B, Dohčević-Mitrović Z, Šćepanović M (2014) Surface modification of sol–gel synthesized TiO_2 nanoparticles induced by La-doping. Mater Charact 88:30–41

Klug HP, Alexander LE (1974) X-ray diffraction procedures: for polycrystalline and amorphous, Secondth edn. Wiley-Interscience Publication, John Wiley & Sons, New York, pp 656–687

Li FB, Li XZ, Hou MF, Cheah KW, Choy WCH (2005) Enhanced photocatalytic activity of Ce^{3+}–TiO_2 for 2-mercaptobenzothiazole degradation in aqueoussuspension for odour control. Appl Catal A: Gen 285:181–189

Liotta LF, Gruttadauria M, Di Carlo G, Perrini G, Librando V (2009) Heterogeneous catalytic degradation of phenolic substrates: catalysts activity. J Hazard Mat 162:588–606

Liqiang J, Xiaojun S, Baifu X, Baiqi W, Weimin C, Honggang F (2004) The preparation and characterization of La doped TiO_2 nanoparticles and their photocatalytic activity. J Solid State Chem 177:3375–3382

Ma HL, Yang JY, Dai Y, Zhang YB, Lu B, Ma GH (2007) Raman study of phase transformation of TiO_2 rutile single crystal irradiated by infrared femtosecond laser. Appl Surf Sci 253:7497–7500

Martins RC, Amaral-Silva N, Quinta-Ferreira RM (2010) Ceria based solid catalysts for Fenton's depuration of phenolic wastewaters, biodegradability enhancement and toxicity removal. Appl Catal B: Environ 99:135–144

Nguyen-Phan T-D, Song MB, Kim EJ, Shin EW (2009) The role of rare earth metals in lanthanide-incorporated mesoporous titania. Micropor Mesopor Mat 119:290–298

Ohsaka T, Izumi F, Fujiki Y (1978) Raman spectrum of anatase, TiO_2. J Raman Spectrosc 7:321–324

Park H, Park Y, Kim W, Choi W (2013) Surface modification of TiO_2 photocatalyst for environmental applications. J Photochem and Photobio C 15:1–20

Patel N, Jaiswal R, Warang T, Scarduelli G, Dashora A, Ahuja BL, Kothari DC, Miotello A (2014) Efficient photocatalytic degradation of organic water pollutants using V–N-codoped TiO_2thin films. Appl Catal B: Environ 150–151:74–81

Peiró AM, Ayllón JA, Peral J, Doménech X (2001) TiO_2-photocatalyzed degradation of phenol and *ortho*-substituted phenolic compounds. Appl Catal B: Environ 30:359–373

Pelaez M, Nolan NT, Pillai SC, Seery MK, Falaras P, Kontos AG, Dunlop PSM, Hamilton JWJ, Byrne JA, O'Shea K, Entezari MH, Dionysiou DD (2012) A review on the visible light active titanium dioxide photocatalysts for environmental applications. Appl Catal B: Environ 125:331–349

Ranjit KT, Willner I, Bosmann SH, Braun AM (2001) Lanthanide oxide-doped titanium dioxide photocatalysts: novel photocatalysts for the enhanced degradation of *p*-chlorophenoxyacetic acid. Environ Sci Technol 35:1544–1549

Sibu CP, Rajesh Kumar S, Mukundan P, Warrier KGK (2002) Structural modifications and associated properties of lanthanum oxide doped sol-gel nanosized titanium oxide. Chem Mater 14:2876–2881

Silva AMT, Silva CG, Dražić G, Faria JL (2009) Ce-doped TiO_2 for photocatalytic degradation of chlorophenol. Catal Today 144:13–18

Sing KSW, Everett DH, Haul RAW, Moscou L, Pierotti RA, Rouquérol J, Siemienewska T (1985) Reporting physisorption data for gas/solid systems. Pure Appl Chem 57:603–619

Sun H, Zhou G, Liu S, Ang HM, Tadé MO, Wang S (2013) Visible light responsive titania photocatalysts codoped by nitrogen and metal (Fe, Ni, Ag, or Pt) for remediation of aqueous pollutants. Chem Eng J231:18–25

Wang X, So L, Su R, Wendt S, Hald P, Mamakhel A, Yang C, Huang Y, Iversen BB, Besenbacher F (2014) The influence of crystallite size and crystallinity of anatase nanoparticles on the photo-degradation of phenol. J Catal 310:100–108

Xiao J, Peng T, Li R, Peng Z, Yan C (2006) Preparation, phase transformation and photocatalytic activities of cerium-doped mesoporous titania nanoparticles. J Solid State Chem 179:1161–1170

Xu Y, Chen H, Zeng Z, Lei B (2006) Investigation on mechanism of photocatalytic activity enhancement of nanometer cerium-doped titania. Appl Surf Sci 252:8565–8570

Yan J, Wu G, Guan N, Li L (2014) Nb_2O_5/TiO_2heterojunctions: synthesis strategy and photocatalytic activity. Appl Catal B: Environ 152–153:280–288

Zhang Q, Gao L, Gou J (2000) Effects of calcination on the photocatalytic properties of nanosized TiO_2 powders prepared by $TiCl_4$ hydrolysis. Appl Catal B: Environ 26:207–215

Zhou G, Sun H, Wang S, Ming Ang H, Tadé MO (2011) Titanate supported cobalt catalysts for photochemical oxidation of phenol under visible light irradiations. Sep Purif Technol 80:626–634